HHS Public Access

Author manuscript

*Biochemistry*. Author manuscript; available in PMC 2018 December 12.

Published in final edited form as:

*Biochemistry*. 2017 December 12; 56(49): 6503–6514. doi:10.1021/acs.biochem.7b00836.

# Deoxycholate-Enhanced *Shigella* Virulence is Regulated by a Rare π-Helix in the Type Three Secretion System Tip Protein IpaD

**Abram R. Bernard**[‡,1], **T. Carson Jessop**[‡,1], **Prashant Kumar**[2], and **Nicholas E. Dickenson**[1,*]

[1]Department of Chemistry and Biochemistry, Utah State University, Logan, UT 84322, USA

[2]Department of Pharmaceutical Chemistry, University of Kansas, Lawrence, KS 66047, USA

## Abstract

Type three secretion systems (T3SS) are specialized nano-machines that support infection by injecting bacterial proteins directly into host cells. The *Shigella* T3SS has uniquely evolved to sense environmental levels of the bile salt deoxycholate (DOC) and upregulate virulence in response to DOC. In this study, we describe a rare i+5 hydrogen bonding secondary structure element (π-helix) within the type three secretion system tip protein IpaD that plays a critical role in DOC-enhanced virulence. Specifically, engineered mutations within the π-helix altered the pathogen's response to DOC with one mutant construct in particular exhibiting an unprecedented reduction in virulence following DOC exposure. Fluorescence polarization binding assays showed that these altered DOC responses are not the result of differences in affinity between IpaD and DOC, but rather differences in the DOC-dependent T3SS tip maturation resulting from IpaD binding the translocator/effector protein IpaB. Together, these findings begin to uncover the complex mechanism of DOC-enhanced *Shigella* virulence while identifying an uncommon structural element that may provide a much needed target for non-antibiotic treatment of *Shigella* infection.

## Graphical Abstract

*To whom correspondence should be addressed: Department of Chemistry and Biochemistry, Utah State University, Logan, UT 84322, 0300 Old Main Hill, Logan, UT 84321, Tel. 435-797-0982, nick.dickenson@usu.edu.

‡Authors contributed equally to this work

Supporting Information Available: Uninduced and Congo red-induced *Shigella* secretion profiles probed with antibodies against IpaB, IpaC, IpaD, and the cytoplasmic control protein glyceraldehyde 3-phosphate dehydrogenase (Supplementary Figure S1), individual far-UV circular dichroism spectra and thermal unfolding profiles for each of the IpaD mutant constructs used in this study (Supplementary Figure S2), fluorescence polarization binding curves between the engineered IpaD mutant constructs and FITC-labeled deoxycholate (Supplementary Figure S3), invasion phenotypes pre and post DOC exposure for *Shigella* strains expressing each of the studied IpaD mutants (Supplementary Figure S4), fluorescence polarization competition profile (Supplementary Figure S5), a table summarizing the predicted secondary structure content and identified secondary structure melt temperatures for each of the purified IpaD constructs used in this study (Supplementary Table S1), and a table summarizing the uninduced protein secretion profiles for each of the *Shigella* strains generated in this study (Supplementary Table S2). The X–Y dataset for Figure 5 is indexed in OpenAIRE, DOI 10.5281/zenodo.1042802.

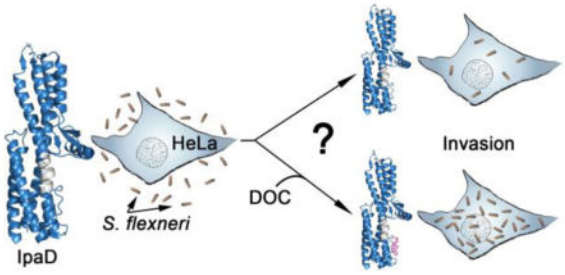


**Keywords**

T3SS; secretion; bile salt; DOC; invasion plasmid antigen; translocon; virulence; enteric; π-bulge; pi-bulge

## Introduction

Infection by *Shigella* spp. results in bacillary dysentery (shigellosis) and represents one of the leading bacterial causes of diarrheal disease worldwide.[2,3] Severe symptoms of shigellosis and an extraordinarily low infectious dose (10–100 organisms)[4] make *Shigella* a significant public health threat resulting in an estimated 90 million infections and 100,000 deaths per year.[5] Infections are primarily spread through the fecal-oral route, driving an especially high mortality rate in developing countries with a lack of clean water supplies and necessary medical care.[5] Furthermore, the children in these regions often suffer frequent infections and infection-related malnutrition leading to declines in childhood growth and cognitive development.[6] While generally better controlled, *Shigella* infections are not uncommon in industrialized nations where the rapid emergence of antibiotic resistant *Shigella* strains make shigellosis a true worldwide threat, underscoring the urgency for better understanding the virulence mechanisms supporting *Shigella* infection.[7,8]

*Shigella* is a Gram-negative facultative anaerobe that employs a type three secretion system (T3SS) as a primary virulence factor.[9,10] Structurally, the type III secretion apparatus (T3SA) is highly conserved among pathogens including *Shigella, Salmonella, E. coli, Yersinia,* and *Burkholderia,* resembling a nano-syringe and needle through which proteins are injected directly from the bacterial cytoplasm into the targeted host cell. Once injected, the effector proteins alter host cell function, support infection, and help the bacteria evade host cell immune responses.[8,11]

The overall structure of the T3SA is quite similar from pathogen to pathogen, however, the specific apparatus details provided below refer to the *Shigella* T3SA. The nascent apparatus is made of three main components including the basal body that anchors the apparatus to the bacterial inner and outer membranes, a hollow needle-like structure that extends beyond the lipopolysaccharide (LPS) layer[12,13] and a pentameric protein tip complex including invasion plasmid antigen D (IpaD).[14,15] From this location at the tip of the needle, IpaD serves as a critical sensor of environmental small molecules such as bile salts, helping to control the structure and composition of the tip complex and secretion of effector proteins.[14,16] The bile salt deoxycholate (DOC) is essential for proper dietary fat solubilization and intestinal

absorption and is found in concentrations as high as 30 mM in human bile.[17] As an enteric pathogen, *Shigella* encounter high concentrations of DOC as they pass through the small intestine en route to the colon. The T3SS tip protein IpaD binds DOC with micromolar affinity,[18] resulting in significant protein conformational changes that support the recruitment of the first hydrophobic translocator, invasion plasmid antigen B (IpaB),[19,20] to the maturing tip complex in preparation of host membrane interaction.[18,19] Upon contact with host membrane components, the second hydrophobic translocator, invasion plasmid antigen C (IpaC), is recruited to the tip of the *Shigella* T3SA.[21] IpaC incorporation into the *Shigella* T3SA completes formation of the translocon pore in the host cell membrane and initiates secretion of effectors into the host cell, promoting pathogen entry.[21]

*Shigella* has provided an invaluable system for following the individual steps involved in T3SA tip complex maturation and helped to shape the current understanding of the apparatus in related pathogens, however, the precise mechanisms and molecular interactions involved in the maturation of the *Shigella* T3SS tip complex remain unclear. Uncovering these mechanisms remains a high priority for understanding of the overall function of the complex T3SS and may ultimately be key in the development of much needed anti-infective agents and vaccines against *Shigella* and related pathogens. We have previously employed several techniques including NMR,[19] FRET,[19,20,22] and high-resolution X-ray crystallography[23] to identify the DOC binding site within IpaD and to determine the structural influence of the interaction on IpaD itself. Alignment of apo-[24] and DOC-bound[23] structures of IpaD (Figure 1) clearly illustrates the global structural influence that DOC binding has on IpaD. The most evident effect is the altered orientation of the central helices with respect to one another and a “bulge” in helix 3 that becomes exaggerated upon binding DOC, allowing the aforementioned conformational changes to occur. The identified “bulge” is a rare form of secondary structure, a π-helix, that results from a localized deviation from the traditional α-helix i+4 backbone hydrogen bonding pattern to i+5 hydrogen bonding in two consecutive positions within the structure (Figure 1).[25,26] In this study, we probed the influence of the π-helix on DOC-mediated *Shigella* T3SA maturation and virulence enhancement by first identifying three residues within the π-helix that are thermodynamically unfavorable in terms of α-helix formation (ΔΔG values 0.31 – 0.68 kcal/mol relative to alanine).[27] The presence of these residues may play important roles in the formation of the π-helix structure and the resulting flexibility in that region. These residues were targeted for mutagenesis and tested for *in vitro* and *in vivo* function, finding that the targeted residues are essential for proper IpaD/IpaB interaction and DOC-enhanced *Shigella* invasion phenotype.

The findings from these studies help tie together several previous works from us and others describing DOC interaction with IpaD and provide valuable mechanistic insight into the role of the identified π-helix in *Shigella* T3SA tip maturation and ultimately the pathogen’s ability to infect host cells.[16,18–20,23] Our hope is that these findings may aid in the development of much needed anti-infective treatments against *Shigella* and perhaps *Salmonella*, which also exhibits a conserved π-helix in its SPI1 T3SS tip protein SipD.

## Experimental Procedures

### Materials

Wild-type (WT) *S. flexneri* corresponds to the serotype 2a 2457T strain originally isolated in 1954.[28] The nonpolar *ipaD* null strain (ΔIpaD) was engineered by Philippe Sansonetti.[29] FITC-deoxycholate and rabbit polyclonal antibodies against IpaB, IpaC, and IpaD were generous gifts from William and Wendy Picking (University of Kansas). *E. coli* strains, the pET15b expression plasmid, and 2X ligation mix were from Novagen (Madison, WI). Restriction enzymes, PCR buffer, and Phusion High-Fidelity polymerase were purchased from New England Biolabs (Ipswich, MA). Oligonucleotide primers were from Integrated DNA Technologies (Coralville, IA). The Superdex 16/600 size exclusion and 5 mL Q FF columns were purchased from General Electric (Pittsburgh, PA). Thiol reactive fluorophores used for selective cysteine labeling were from Thermo Fisher Scientific (Waltham, MA). Defibrinated sheep red blood cells were from Colorado Serum Company (Denver, CO). All other solutions and chemicals were of reagent grade.

### Cloning

Wild-type *ipaD* and *ipaB* genes were amplified from the isolated virulence plasmid of *S. flexneri* 2457T using primers to generate restriction sites that allowed insertion into pET15b, pWPsf4, and pT7HMT expression plasmids. The truncated gene encoding the soluble IpaB construct, $IpaB^{28–226}$, was previously generated within the pT7HMT construct using inverse PCR.[20] The *ipaD* π-helix alanine mutants in pET15b and pWPsf4 were similarly generated in the respective vectors using inverse PCR. All sequences were verified by Sanger sequencing prior to transformation into chemically competent *E. coli* using the manufacturer's recommended heat shock protocol or electro-competent *S. flexneri* strains via electroporation.

### Protein expression and purification

Wild-type *ipaD* and the seven π-helix *ipaD* point mutants in pET15b were transformed into *E. coli* Tuner (DE3) cells (Novagen). Each strain was grown overnight in Luria-Bertani (LB) media containing 0.1 mg/mL ampicillin to maintain the expression plasmid. Two milliliters of the overnight cultures were used to inoculate 500 mL of Terrific Broth (TB) media containing 0.1 mg/mL ampicillin prior to incubation at 37 °C and 200 rpm. Once the cultures reached an optical density ($OD_{600}$) of 0.8, they were cooled to 17 °C and protein expression was induced with the addition of isopropyl-β-D-1-thiogalactopyranoside (IPTG) to a final concentration of 1 mM. The cultures continued to incubate at 17 °C and 200 RPM for 18–24 hours. $IpaB^{28–226}$ pT7HMT protein expression was carried out identically as described above for IpaD, but the media contained 0.05 mg/mL kanamycin in place of ampicillin. Following the 18–24 hour protein expression period, the cells were harvested via centrifugation, resuspended in binding buffer (20 mM Tris, 500 mM NaCl, 5 mM imidazole, pH 7.9) containing 0.2 mM 4-(2-aminoethyl) benzenesulfonyl fluoride hydrochloride (AEBSF), and lysed using a probe sonicator. The resulting lysate was clarified by high-speed centrifugation and each of the expressed proteins were initially purified via their N-terminal 6x-Histidine tags using nickel chelation chromatography. The IpaD proteins were further purified using anion exchange chromatography (GE 5 mL HiTrap Q FF Column)

followed by dialysis into PBS pH 7.4. The nickel-purified IpaB$^{28–226}$ was concentrated using an Amicon Ultra 15 centrifugal filter unit with a 30-kDa molecular weight cutoff and further purified using a GE Superdex 200 16/600 size exclusion column equilibrated with PBS, pH 7.4. All purified protein fractions were evaluated using SDS-PAGE, stored at 4 °C, and used within one week, though they appeared to remain stable much longer.

### Far-UV Circular Dichroism (CD)

Far-UV CD spectra and secondary structure thermal stability profiles were collected for wild-type IpaD and each of the engineered IpaD mutants in the absence and presence of 1 mM DOC. All data were collected using a JASCO model J-1500 spectropolarimeter equipped with a temperature controlled sample chamber. CD spectra were collected from 200 nm to 260 nm at 10 °C using 0.1 cm quartz cuvettes, 0.5 nm data sampling, a 50 nm/min scan rate, and a 1 sec data integration time. Secondary structure thermal stability profiles were collected in the same 0.1 cm quartz cuvettes by monitoring the CD signal at the 222 nm minimum while the solution temperature was increased from 10 °C to 90 °C at a rate of 0.3 °C/min. Measurements were performed at 0.3–0.6 mg/mL protein concentration and CD signals were normalized by converting to mean residue molar ellipticity. Spectral analysis was performed using the Dichroweb software package and K2D reference set to quantify protein secondary structure content.[30,31] Thermal unfolding transition temperatures (Tm) were determined by plotting the derivative of each thermal stability curve and identifying the corresponding local maxima of the derivative.

### IpaD FITC-DOC Fluorescence Polarization

Fluorescence polarization has previously been used to show that FITC-DOC binds IpaD with micromolar affinity and that the interaction is specific and reversible when titrated with un-labeled DOC.[18] A modified version of this assay was used to determine the effect of the engineered IpaD point mutants on the interaction between IpaD and FITC-DOC. Specifically, 25 nM FITC-DOC was incubated for 30 minutes at 23 °C with increasing concentrations of each of the individual IpaD mutants (0 - 30 μM IpaD) in PBS and transferred to low-binding opaque 96 well flat bottom plates. Fluorescence polarization of the FITC-labeled DOC was measured using a Synergy H4 fluorescence plate reader equipped with polarizers and bandpass filters providing 485 ±10 nm excitation and detection of fluorescence emission at 528 ± 10 nm. Change in polarization relative to that of FITC-DOC alone was plotted as a function of IpaD concentration. The apparent dissociation constant ($K_d$) for each interaction was determined by fitting the raw data to a single site saturation binding model in SigmaPlot 12.

### Effects of directed IpaD π-helix point mutants on Shigella translocator secretion

IpaD is known to reside at the tip of the *Shigella* T3SA[14,32] where it plays a critical role in controlling secretion of subsequent T3SS proteins, including the translocators IpaB and IpaC.[14,33] To determine the effect of the engineered IpaD mutations on translocator expression and secretion profiles in *S. flexneri*, the *ipaD* null *S. flexneri* strain (ΔIpaD) was complemented with each of the engineered IpaD mutants and grown overnight in tryptic soy broth (TSB) containing 0.1 mg/mL ampicillin and 0.05 mg/mL kanamycin. The bacteria were gently separated from the culture supernatant via centrifugation and the soluble,

secreted proteins were isolated by precipitation in the presence of 5% trichloroacetic acid (TCA) followed by centrifugation at 20,000 x g. The resulting protein pellet was washed with acetone, resuspended in SDS sample buffer (210 mM Tris pH 6.8, 100 mM NaCl, 3 mM EDTA, 200 mM SDS, 3 mM $NaN_3$, 0.03% Bromophenol Blue, 30% Glycerol), separated by SDS-PAGE, and transferred to polyvinylidene fluoride (PVDF) membranes. The relative levels of the secreted *Shigella* T3SS translocator proteins IpaB and IpaC were determined using primary antibodies against the proteins followed by Alexa647 conjugated anti-rabbit secondary antibodies. The membranes were visualized using a BioRad ChemiDoc fluorescence imager and protein band intensities quantified via fluorescence densitometry. The relative levels of IpaB and IpaC remaining within the bacterial cells were determined by lysing the isolated bacteria using SDS sample buffer, separating the cellular proteins by SDS-PAGE, transferring to PVDF membranes, and detecting with the same primary and secondary antibody combinations described above. A monoclonal antibody against the cytoplasmic enzyme glyceraldehyde 3-phosphate dehydrogenase was used as a control in the western blot to ensure that the proteins observed in the supernatant were secreted from the bacteria and not the result of cell lysis (Supplementary Figure S1).

The effect of the engineered IpaD π-helix mutations on type three secretion system activation was tested using an established Congo red induction assay that mimics the natural activation of the T3SS by inducing secretion of effector proteins from *S. flexneri*.[34] The protocol is described in detail elsewhere,[35] but briefly *S. flexneri* expressing wild-type IpaD or one of the IpaD mutants were grown overnight on tryptic soy agar (TSA)-Congo red plates and a small number of isolated colonies were used to inoculate 10 mL of TSB containing appropriate antibiotics. The cultures were grown to an $OD_{600}$ of 1.0. The cultures were then cooled and collected via centrifugation at 4 °C prior to resuspension in 500 μL cold Sodium Phosphate buffer, (12 mM $Na_2HPO_4$ or $NaH_2PO_4$, 140 mM NaCl, pH 7.2). Congo red solution was added to a final concentration of 0.3 mg/mL and the bacterial solutions were incubated at 37°C for 10 minutes to induce protein secretion. Following incubation, the mixtures were centrifuged at 14,000 x g for 15 minutes at 4 °C to separate the bacteria from the secreted proteins. A sample of the supernatant for each *S. flexneri* strain was separated by SDS-PAGE, transferred to PVDF membranes, and quantified using anti-IpaB and anti-IpaC antibodies as described above. A monoclonal antibody against the cytoplasmic enzyme glyceraldehyde 3-phosphate dehydrogenase was used as a control in the western blot to ensure that the proteins observed in the supernatant were secreted from the bacteria and not the result of cell lysis (Supplementary Figure S1).

## Contact-mediated hemolysis

The effects of the engineered IpaD mutations on contact-mediated hemolysis of red blood cells was determined using a modified method of one described previously.[36] Briefly, *S. flexneri* expressing wild-type IpaD or one of the IpaD π-helix mutants were grown overnight on TSA-Congo red plates and a small number of isolated colonies were used to inoculate 10 mL of TSB containing appropriate antibiotics. The cultures were grown to an $OD_{600}$ of 1.0, collected by centrifugation, and gently resuspended in 200 μL PBS. Fifty microliters of each bacterial mix was combined with approximately $5x10^8$ red blood cells in a 96 well microtiter plate and centrifuged at 2300 x g and 30 °C for 15 minutes to initiate

contact between the bacteria and the red blood cells. The plate was then incubated at 37 °C for 1 hour prior to the addition of 100 μL cold PBS and resuspension by pipetting. The resuspended mix was centrifuged at 2300 x g and 10 °C for 15 minutes to separate the bacteria, red blood cells, and red blood cell membranes from the released hemoglobin. One hundred microliters of the supernatant was transferred to another 96 well plate and the released hemoglobin quantified by measuring absorbance at 545 nm.

### Bacterial invasion of epithelial cells

*S. flexneri* invasion of cultured HeLa cells was monitored by a gentamicin protection assay as previously described.[37] Sterile 24-well plates were seeded with passaged HeLa cells and grown overnight in DMEM supplemented with 10% fetal calf serum, penicillin, and streptomycin at 100% relative humidity, 37 °C, and 5% $CO_2$. The *S. flexneri* strains tested were streaked onto TSA plates containing 0.025% Congo red and grown overnight at 37 °C. A small number of isolated colonies from each plate were used to inoculate 10 mL of TSB containing appropriate antibiotics to maintain the transformed plasmid. The cultures were grown to an $OD_{600}$ of approximately 0.4 at 37 °C and 200 RPM. Each culture was split with half transferred to a sterile flask containing sodium deoxycholate (final concentration 1 mg/mL). The split cultures were grown an additional 30 minutes before equivalent bacterial loads were introduced to the cultured HeLa cells, which had been rinsed with an antibiotic free 0.45% glucose DMEM solution. The plates were centrifuged at 1000 x g to synchronize contact between the bacteria and HeLa cells prior to incubation at 37 °C for 30 min. Each well in the plate was then rinsed to remove the majority of the extracellular bacteria. The remaining *Shigella* that had not successfully invaded the HeLa cells were selectively killed by treatment with 50 μg/mL gentamicin. Bacteria that had invaded HeLa cells were visualized by lysing the host cells with 1% agarose in water and overlaying with a 2x LB agar solution. Overnight incubation at 37 °C resulted in bacterial colony formation that was quantified and used to provide relative levels of invasiveness between the tested *S. flexneri* strains and directly compare the sensitivity of each strain to DOC exposure.

### Measurement of DOC dependent IpaB-IpaD interactions

The binding affinity between each of the engineered IpaD alanine mutants and the stable $IpaB^{28–226}$ construct was measured using fluorescence polarization much as it was described above for measuring DOC binding to IpaD. We previously engineered the $IpaB^{28–226}$ peptide to contain a single N-terminal cysteine to which an Alexa568 fluorophore was bound through maleimide chemistry, allowing fluorescence polarization measurements to quantify the binding affinity between IpaD and IpaB in the presence and absence of DOC. Here, the DOC effect on binding affinity between IpaB and the engineered IpaD **π**-helix mutants was quantified by holding $IpaB^{28–226}$-Alexa568 concentration constant at 80 nM while the concentration of IpaD or engineered IpaD mutant was titrated from 0–10 μM with identical conditions then tested in the presence of 1 mM DOC. The polarization values under each condition were collected using a Synergy H4 fluorescence plate reader equipped with motorized polarizers and appropriate filter sets. The change in polarization relative to that of $IpaB^{28–226}$-Alexa568 alone DOC was plotted as a function of IpaD concentration in the presence and absence of DOC. The apparent dissociation constant ($K_d$) for each interaction was determined by fitting the data to a single site saturation binding model in SigmaPlot 12.

A binding-site competition assay was additionally performed to ensure that the observed binding under DOC conditions was specific to the ligand and not a result of the introduced fluorophore. For this competition assay, 3.5 μM IpaD was incubated with 80 nM $IpaB^{28–226}$-Alexa568 in the presence of 1 mM DOC prior to the addition of 0–16 μM $IpaB^{28–226}$-Ncys that does not contain a fluorescent label. These results were also fit to a single site saturation binding model with the observed decrease in polarization plotted as a function of unlabeled $IpaB^{28–226}$. The observed decrease in polarization corresponds to the competitive removal of the labeled IpaB peptide from IpaD.

## Results

### Targeting IpaD π-helix residues for mutational analysis

We have previously employed several techniques including NMR,[19] FRET,[19,20] and high-resolution X-ray crystallography[23] to determine the structural effects of DOC binding on IpaD. Alignment of high-resolution apo-[24] and DOC-bound[23] structures of IpaD clearly illustrates the global structural influences that DOC binding has on IpaD (Figure 1). The most noticeable influences are observed in the relative positioning of the two long central helices (α3 and α7) and in the region of the identified π-helix in α3. The π-helix appears to act like a molecular hinge, adopting a more angled geometry upon binding DOC. FRET and fluorescence polarization assays have previously suggested that these DOC-induced conformational changes may be necessary to support the interaction between IpaD and the first translocator protein, IpaB, preparing the T3SA for contact with host cell membranes and ultimately cellular invasion.[21,38] To better understand the mechanistic details of how DOC affects IpaD, we looked at the IpaD primary structure within the region of the π-helix. We found three residues within the region that are thermodynamically unfavorable in terms of α-helix formation and predicted that the deviation from α-helical structure is what permits the necessary DOC-induced conformational changes within this region. The identified residues (D144, N146, and Y149) were each mutated individually and in all permutations to alanine(s) because of alanine's thermodynamic favorability with respect to α-helix formation.[27] The engineered mutants were first expressed in *E. coli* and purified using an N-terminal histidine tag, resulting in protein expression levels and protein purities that are consistent with wild-type IpaD (data not shown). Secondary structure content and stability were examined by circular dichroism for recombinant wild-type IpaD and each of the IpaD π-helix mutants used in the study. The far-UV CD spectra are nearly superimposable for each of the engineered IpaD mutants both in the absence and presence of 1mM DOC, suggesting that the overall secondary structure of the proteins was not adversely affected by the mutations (Figure 2A and Supplementary Figure S2). In addition to empirical analysis, each CD spectrum was analyzed for secondary structure content, finding that each of the mutants maintain approximately 68% α-helix, 2–5% β-sheet, and 24–29% random coil secondary structure (Supplementary Table S1), consistent with the solved structures of both apo- and DOC-bound IpaD. Additionally, CD thermal unfolding profiles monitoring CD signal at 222 nm as a function of temperature found that the thermal stabilities of the mutants were similar to that of wild-type IpaD with dominant transitions from ~73 – 78 °C in the absence of DOC and a trend toward lower transition temperature of each construct in the presence of DOC (Figure 2B, Supplementary Figure S2 and Supplementary Table S1).

This observed decrease in transition temperature in the presence of DOC is consistent with protein binding to a small amphipathic bile salt and appears to be specific as exposure to 1mM concentrations of the bile salt analog dehydrocholate (DHC) does not affect the secondary structure content or thermal stability of IpaD (data not shown), consistent with the inability of DHC to bind IpaD[18]. A fluorescence polarization assay confirmed that the incorporated π-helix mutations did not affect the ability of IpaD to bind DOC. Specifically, a synthetic fluorescein-DOC construct was incubated with increasing concentrations of each of the IpaD mutants and the polarization values for each condition were determined using a fluorescence plate reader. As the small fluorescently labeled DOC ligand binds to IpaD, the rotational diffusion rate of the bound ligand decreases significantly, resulting in an increase in the measured polarization value. Plotting the change in polarization as a function of IpaD/mutant concentration provided similar binding curves for each of the IpaD constructs and apparent dissociation constants ranging from 8.2 ± 2.2 μM to 10.9 ± 0.2 μM (Table 1 and Supplementary Figure S3), confirming that all of the mutants are able to bind DOC similarly to wild-type IpaD (9.3 ± 1.8 μM).

## IpaD π-helix mutants are competent for Shigella secretion induction and regulation

IpaD resides at the tip of the nascent needle[14,32] and is involved in preventing premature protein secretion through the apparatus in addition to triggering apparatus maturation following DOC interaction.[14,20] We examined the ability of each *ipaD* π-helix mutant to restore secretion control and translocon pore formation to the ΔIpaD *Shigella flexneri* strain.

*Shigella* strains lacking *ipaD* are avirulent, at least in part due to the loss of secretion control through the incomplete T3SA.[29,32,33] A comparative analysis of uninduced protein secretion (leakage) and cytoplasmic protein levels of IpaD and the translocator proteins IpaB and IpaC is shown in Figure 3. The western blot signals were quantified and scaled to the ΔIpaD strain complemented with wild-type *ipaD* (Figure 3B and 3C) and the relative secretion levels compared to detected cytoplasmic stores (Supplementary Table S2). As shown previously, high levels of IpaB and IpaC were secreted from the ΔIpaD strain (~250% and ~175%, respectively), confirming a loss of secretion regulation in the absence of IpaD. Complementation of the ΔIpaD strain with wild-type *ipaD*, or any of the *ipaD* π-helix mutants, reduced T3SS leakage to less than or equal to wild-type levels (one-way ANOVAs comparing secretion levels of IpaB, IpaC and IpaD to wild-type levels of the corresponding protein; followed by a Dunnett's post test, $p \leq 0.01$).

The ability of the *IpaD* π-helix *Shigella* mutants to actively secrete translocator proteins was examined using an established Congo red secretion assay (Figure 4). Congo red is a small molecule dye that activates the *Shigella* T3SS, initiating secretion of proteins including IpaB and IpaC, among others.[34] The *Shigella* mutants were exposed to Congo red, the supernatant containing secreted proteins was collected, and the levels of secreted IpaD, IpaB and IpaC quantified by western blot (Figure 4A and 4B). Each of the engineered mutants supported Congo red induced T3SS activation as observed by secreted IpaB and IpaC levels similar to those of the strain expressing wild-type IpaD. IpaC secretion levels were particularly sensitive to Congo red activation with each of the engineered IpaD π-helix mutants showing

a significant increase in secretion levels compared to the *ipaD* null strain (one-way ANOVA followed by a Dunnett's post test, $p \leq 0.01$).

In addition to secretion regulation, IpaD also serves as the platform for the hydrophobic translocon pore that resides at the tip of the mature T3SA and spans the membrane of targeted host cells.[38–41] Contact-mediated hemolysis quantifies the efficiency of pore formation through detection of hemoglobin released from red blood cells compromised by T3SS translocon insertion.[36] Table 2 includes the results of the contact-mediated hemolysis assay in which *e*ach of the seven mutant *Shigella* strains exhibited hemolysis levels similar to the *Shigella* strain expressing wild-type IpaD (one-way ANOVA ($F(7,16) = 2.785$, $p = 0.043$)). This confirms that each of the engineered IpaD π-helix *Shigella* strains is capable of responding to cell membrane contact and that their T3SA can support translocon formation but the more sensitive gentamycin protection assay is required to uncover the influence of DOC interaction with the IpaD π-helix mutants on *Shigella* virulence.

## The identified π-helix in IpaD regulates IpaD/IpaB interaction and is critical for DOC enhancement of cellular invasion

The *Shigella* secretion and hemolysis assays described above provide a sensitive means of evaluating the effects of the engineered IpaD π-helix mutations on secretion regulation and ability to support translocon formation, respectively. Technical limitations of these assays, however, prevent them from observing effects resulting from deoxycholate exposure, requiring a gentamicin protection assay to specifically probe for DOC effects. A gentamicin protection assay was used to quantify the invasion capabilities of the *ipaD* mutant *S. flexneri* strains, mimic the environment that the pathogen experiences in the small intestine during a normal course of infection, and uncover the influence of the engineered IpaD π-helix mutants on DOC-enhancement of invasion phenotype. Table 2 and Supplementary Figure S4 provide the quantitated results of cellular invasion scaled to the wild-type *ipaD* complemented ΔIpaD strain. The response to DOC is included as the percent increase in invasion observed following DOC exposure for each strain. While the *ipaD* null strain is completely non-invasive, complementation with wild-type *ipaD* or any of the *ipaD* π-helix mutants at least partially restored invasion phenotype. In fact, in the absence of DOC, the invasion phenotype of many of the IpaD π-helix mutants were not statistically different from that of the wild-type *ipaD* complemented strain (one-way ANOVA followed by a Dunnett's post test, $p \leq 0.01$)). The *ipaD*$^{D144A}$ strain exhibited 142 ± 28% relative invasion compared to the wild-type *ipaD* complement while the *ipaD*$^{N146A}$ and *ipaD*$^{N146A/Y149A}$ strains were only 78 ± 25% and 68 ± 7% invasive, respectively. Given the predicted role of the IpaD π-helix in DOC-mediated *Shigella* virulence enhancement, however, the more interesting experiment tested the effect the mutations had on *Shigella* invasion following DOC exposure. As expected, DOC exposure resulted in an 83 ± 14% increase in the invasiveness of the *Shigella* strain expressing wild-type IpaD. However, some of the IpaD π-helix mutants showed much different sensitivities to DOC exposure (Table 2 and Supplementary Figure S4). For example, while the strain expressing IpaD$^{D144A/Y149A}$ displayed essentially wild-type invasion levels in the absence of DOC (85 ± 38%), it only exhibited a 39 ± 15% increase in invasion following DOC exposure, suggesting the mutation reduced the sensitivity of the T3SS to DOC (one-way ANOVA followed by a Dunnett's post test, $p \leq$

0.01)). On the other hand, the strain expressing IpaD$^{D146A}$ was found to be deficient in both invasion capability and response to DOC with a 78 ± 25% invasion phenotype in the absence of DOC and a reduced sensitivity to DOC resulting in a modest 50 ± 35% increase in invasion. Most unexpectedly, however, we found that while the strain expressing the IpaD$^{D144A/N146A/Y149A}$ triple mutant showed wild-type invasion levels in the absence of DOC, it resulted in an unprecedented 28 ± 20% decrease in invasion following DOC exposure.

It is clear that *Shigella* exposure to DOC mobilizes the translocator protein IpaB to the tip of the T3SA where it interacts with IpaD and forms a stable oligomeric pre-pore complex.[18,20] Additionally, we have previously shown that *in vitro* binding between IpaD and a soluble IpaB construct (IpaB$^{28–226}$) requires the addition of DOC and that binding is accompanied by conformational changes in IpaD that are consistent with the significant flexibility afforded by the identified π-helix.[23] To bridge the gap between these findings and the observed differences in DOC effect on *Shigella* invasion phenotype among the IpaD π-helix mutants, we implemented a fluorescence polarization assay to quantify the binding affinity between the engineered IpaD mutants and the translocator protein IpaB. Fluorescence polarization binding curves between the fluorescein-labeled soluble IpaB$^{28–226}$ construct and each of the engineered IpaD π-helix mutants were generated in the absence and presence of DOC and compared to wild-type IpaD (Figure 5). The binding data were fit to a single site saturation model, providing apparent $K_d$ values for each interaction and finding that wild-type IpaD was unable to appropriately interact with IpaB$^{28–226}$ in the absence of DOC (determined by a significantly attenuated overall change in polarization and inability of the data to be fit by the binding model ($R^2 \leq 0.95$).

Subsequent addition of DOC supported binding of the labeled IpaB construct to IpaD with an apparent dissociation constant of 2.0 ± 0.7 μM. Competition with unlabeled IpaB$^{28–226}$ displaced the labeled construct, ensuring specificity of the interaction (Supplementary Figure S5). Furthermore, we found that DOC was required for the interaction between IpaB$^{28–226}$ and all but one of the IpaD π-helix mutants, resulting in affinities ranging from 0.3 ± 0.2 μM to 2.2 ± 0.8 μM (Table 3). Unexpectedly, the IpaD$^{D144A/N146A/Y149A}$ triple mutant efficiently bound IpaB in the absence of DOC with an apparent binding constant of 7.4 ± 2.4 μM, suggesting that mutation of the three targeted π-helix residues together either mimics the DOC-bound conformation of IpaD or perhaps provides the conformational flexibility necessary for IpaD to bind IpaB *in vitro*. It should be noted, however, that in either case, the interaction still benefits from the addition of DOC as the affinity was increased to 2.2 ± 0.8 μM following DOC exposure. The precise relationship between the effects of the π-helix mutations observed for IpaD/IpaB interaction and invasion phenotype enhancement remain somewhat unclear. We hypothesize, however, that the π-helix mutations provide additional structural flexibility that supports the observed *in vitro* increase in affinity for IpaB in the absence of DOC while restraints within the IpaD pentamer at the tip of the MxiH needle may ultimately result in unfavorable conformations following DOC binding *in vivo,* ultimately resulting in the observed decrease in invasion phenotype of the triple mutant following DOC exposure.

## Discussion

The findings presented in this study uncover the importance of the IpaD π-helix in *Shigella's* virulence response to DOC as well as providing the first demonstration of DOC-independent IpaD/IpaB interaction *in vitro*, beginning to uncover the mechanism driving *Shigella* T3SA maturation and preparation for host cell infection. Ultimately, complex computational studies and high-resolution structures of isolated and complexed T3SA components will be required to fill in the remaining gaps regarding T3SS function with respect to DOC sensitivity, however, this work provides a strong foundation for these studies and will hopefully lead to much needed anti-infective treatments against the broad range of pathogens that harbor type three secretion systems.

Type three secretion systems are nano-machines that uniquely transport bacterial effector proteins across three membranes (two bacterial and one host) to reach the host cell cytoplasm, subverting host function and ultimately supporting infection.[42–44] While the overall structure of the type three secretion apparatus is highly conserved among a diverse set of plant, animal, and human pathogens, insight into specific structural and mechanistic differences is beginning to help us understand how each pathogen functions in its own niche environment.[45] Here, for example, we characterized a prominent π-helix located in the *Shigella* tip protein IpaD, finding that it is critical in supporting bile salt-mediated enhancement of *Shigella* virulence. When the available structures of the T3SS tip proteins from *Burkholderia pseudomallei,*[46] *Yersinia pestis*,[47] and *Salmonella enterica* serovar Typhimurium[48] (BipD, LcrV, and SipD, respectively) are evaluated and compared to the structure of IpaD,[24] only the *Salmonella enterica* protein SipD exhibits a canonical π-helix structure as seen in IpaD (Figure 6). Both BipD and LcrV maintain traditional i+4 hydrogen bonding patterns throughout the length of their central helices.

The π-helix secondary structure element identified in IpaD (and SipD) has also been referred to in other proteins as a π-bulge, α-aneurism, or looping out, but in all cases, is defined by at least two consecutive π-type i+5 hydrogen bonds that in many proteins results in an observed discontinuity within a traditional α-helix surrounding the π-helix element.[25,26] The bonding pattern that results from incorporating a π-helix provides an increase in Gibbs free energy of approximately 3–6 kcal/mol,[49,50] explaining why it is rare to observe π-helices in protein structures and why those that are found are generally associated with critical function(s).

Thorough discussions concerning the roles and evolutionary implications of π-helices in specific proteins can be found elsewhere,[25,26] however, it is important to note that π-helices are critical to the function of a diverse set of proteins and it is likely that the known cases only represent a fraction of what exists. For example, a short α- to π-helix transformation in the *E. coli* glucosyltransferase OtsA provides the non-linear geometry necessary to orient an essential tryptophan sidechain into the binding pocket for the coenzyme PLP.[25,51] Additionally, Cooley et al. found that ligand-induced conformational changes within the hydroxylase component of methane monooxygenase are driven by peristaltic-like shifts in active site π-helices with similar results seen upon binding of a regulatory protein subunit to the related toluene-4-monooxygenase hydroxylase.[25,52] In the latter example, the π-helices

appear to translate the binding of the regulatory protein subunit to the active site, much as we propose is happening upon DOC binding to the *Shigella* protein IpaD.

Stensrud et al. first showed that the bile salt deoxycholate binds specifically to IpaD[18] with micromolar affinity and we later used NMR and FRET to show that DOC binding results in significant conformational changes within IpaD and that these DOC-induced conformational changes support a stable interaction between IpaD and the T3SS translocator protein IpaB.[19,20] It was not until later when we solved the DOC-bound IpaD structure, however, that the importance of the structural flexibility provided by the π-helix in IpaD became apparent.[23] Upon binding DOC, the π-helix acts as a hinge driving the constriction of the two central helices (α3 and α7) relative to one another and supporting a nearly 8 Å movement of the proximal end of α7 relative to the apo-structure.[5] In this study, we have shown that targeted mutations within the π-helix did not abrogate the secretion capabilities of the *Shigella* T3SS or the ability of *Shigella* to infect host cells, however, the mutants did provide compelling results with respect to sensitivity to DOC. The *Shigella* strain expressing the IpaD$^{D144A/N146A/Y149A}$ mutant lost DOC-based enhancement of host cell invasion and in fact exhibited an unprecedented reduction in virulence following DOC exposure. Additionally, the same IpaD mutant also represents the only engineered IpaD construct capable of binding the translocator protein IpaB regardless of DOC conditions, suggesting that the mutations in the π-helix either altered the overall IpaD structure to more closely mimic that of DOC bound IpaD, or perhaps provided the additional structural flexibility necessary to support the IpaD/IpaB interaction. It is additionally worth noting that while none of the π-helix mutations except the triple mutant resulted in DOC-independent IpaD/IpaB interaction, most of the engineered IpaD mutants did result in higher affinity for IpaB in the presence of DOC (Table 3 and Figure 5). These results suggest that some of the π-helix mutations provide favorable conformations or additional flexibility to IpaD even following DOC binding, though mutation of all three targeted residues was required to mitigate the need for DOC to support IpaD-IpaB interaction.

These data and others presented in this study expand on previous work from ourselves and others to uncover a specialized role for the IpaD π-helix in which IpaD serves as an environmental sensor for DOC capable of translating ligand binding to conformational changes that support IpaB recruitment and stable interaction at the T3SA tip. This recruitment of IpaB serves as the first active step in the maturation of the tip complex and prepares *Shigella* for host cell contact and invasion of the colonic epithelium. Given that *Shigella* is strictly an enteric pathogen and that it specifically targets the large intestine for infection, it makes sense that it would exploit the high levels of DOC found in the small intestine to essentially provide a biological landmark and ensure that the pathogen is only fully prepared for invasion just prior to reaching the colon. In contrast, while *Burkholderia pseudomallei* is also a T3SS-expressing human pathogen, infection is generally initiated by direct environmental contact and there is little chance of bile salt exposure during infection,[53] perhaps explaining the inability of BipD to bind DOC[18] and the lack of π-helices in the protein structure (Figure 6). Similarly, human infection by *Yersinia pestis* results from direct transfer of the pathogen from a flea vector into the bloodstream of the host, bypassing intestinal and bile salt exposure,[54] again perhaps explaining why LcrV from *Y. pestis* does not contain any apparent π-helices. Infection from either *Yersinia*

*enterocolitica* or *Yersinia pseudotuberculosis*, on the other hand, often results from consumption of contaminated food.[53] As a result, they do encounter similar host environments as *Shigella* and may in fact benefit from bile salt sensitivity. Unfortunately, no specific bile salt sensitivity assays have been performed and no structures exist for LcrV from these species to identify such an interaction or provide much needed structural comparisons. Additionally, while sequence alignments of LcrV from *Y. pestis*, *Y. enterocolitica* and *Y. pseudotuberculosis* share 91% sequence identity and do not exhibit sequence deviations one would predict to provide π-helices within LcrV of the enteric Yersinia species, π-helices are notoriously difficult to identify a priori and it remains likely that high-resolution structures will be required to ultimately answer this question. Finally, perhaps the most interesting IpaD homolog to consider with respect to bile salt response is SipD from *Salmonella enterica.* Much like *Shigella spp.*, *S. enterica* is an enteric pathogen with infection most often resulting from consumption of contaminated food or water. Once ingested, the bacteria pass through the small intestine where they rely on two independent type three secretion systems to invade the colonic epithelium and escape the endocytic vacuole to access the blood and lymphatic systems.[55,56] Prouty and colleagues published a series of studies showing that *Salmonella* grown in the presence of DOC exhibit reduced invasion phenotypes and that deoxycholate plays a strong role in *Salmonella* transcriptional regulation.[57–59] Specifically, DOC binds the repressor MarR, upregulating transcription of the *marRAB* operon responsible for multiple antibiotic resistance and independently activating transcription of the genes encoding the AcrAB efflux pump.[57] In the context of the *Salmonella* T3SS, crystal structures of SipD confirm the presence of a π-helix as well as a specific binding site for DOC.[48] In contrast to IpaD, however, the affinity of SipD for DOC is significantly reduced[18] and DOC binding does not result in notable conformational changes within the protein[48] or any reports of altered pathogen virulence, leaving the role of DOC binding to SipD unclear. Based on the results presented here, it is tempting to speculate that the observed T3SS π-helices evolved as a means to permit DOC sensing by pathogens whose primary infection pathways pass through the small intestine, however *Shigella* currently represents the only T3SS encoding pathogen for which a comprehensive characterization, with respect to DOC, has been performed. Similar work with additional enteric pathogens such as *S. enterica*, *E. coli*, *Y. pseudotuberculosis*, and *Y. enterocolitica* will shed light on the evolutionary role of π-helices in T3SS and help to better define environmentally driven diversification of T3SSs in general.

## Supplementary Material

Refer to Web version on PubMed Central for supplementary material.

## Acknowledgments

**Funding Source Statement:** This work was supported, in part by grants from the NIH (1K22AI099086-01A1 and 1R15AI124108-01A1) and R. Gaurth Hansen endowment funds to N.E.D., a Utah State University Presidential Doctoral Research Fellowship (PDRF) to A.R.B., and a Utah State University Undergraduate Research and Creative Opportunities (URCO) Grant to T.C.J.

We thank William Picking and Wendy Picking (University of Kansas in Lawrence, KS) for access to the CD spectropolarimeter and for technical discussions.

## Abbreviations

| | |
|---|---|
| **AEBSF** | 4-(2-aminoethyl) benzenesulfonyl fluoride hydrochloride |
| **CD** | circular dichroism |
| **DMEM** | Dulbecco's Modified Eagle's medium |
| **DOC** | deoxycholate |
| **FM** | fluorescein maleimide |
| **FP** | fluorescence polarization |
| **FRET** | Förster resonance energy transfer |
| **IpaB** | Invasion plasmid antigen B |
| **IpaC** | Invasion plasmid antigen C |
| **IpaD** | invasion plasmid antigen D |
| **LB** | Luria-Bertani |
| **LPS** | lipopolysaccharide |
| **NMR** | nuclear magnetic resonance |
| **PDVF** | polyvinylidene fluoride |
| **PBS** | phosphate buffered saline |
| **T3SA** | type III secretion apparatus |
| **T3SS** | type three secretion system |
| **TB** | terrific broth |
| **TCA** | trichloro acetic acid |
| **TSB** | tryptic soy broth |

## References

1. The PyMOL Molecular Graphics System, version 1.8. Schrödinger, LLC;
2. Kotloff KL. The Burden and Etiology of Diarrheal Illness in Developing Countries. Pediatr Clin North Am. 2017; 64:799–814. [PubMed: 28734511]
3. Troeger C, Forouzanfar M, Rao P, Khalil I, Brown A, Reiner RCJ, Fullman N, Thompson RL, Abajobir A, Ahmed M, Alemayohu MA, Alvis-Guzman N, Amare AT, Antonio CA, Asayesh H, Avokpaho E, Awasthi A, Bacha U, Barac A, Betsue BD, Beyene AS, Boneya DJ, Malta DC, Dandona L, Dandona R, Dubey M, Eshrati B, Fitchett JRA, Gebrehiwot TT, Hailu GB, Horino M, Hotez PJ, Jibat T, Jonas JB, Kasaeian A, Kissoon N, Kotloff K, Koyanagi A, Kumar GA, Rai RK, Lal A, El Razek HMA, Mengistie MA, Moe C, Patton G, Platts-Mills JA, Qorbani M, Ram U, Roba HS, Sanabria J, Sartorius B, Sawhney M, Shigematsu M, Sreeramareddy C, Swaminathan S, Tedla BA, Jagiellonian RT, Ukwaja K, Werdecker A, Widdowson MA, Yonemoto N, El Sayed Zaki M, Lim SS, Naghavi M, Vos T, Hay SI, Murray CJL, Mokdad AH. Estimates of global, regional, and

national morbidity, mortality, and aetiologies of diarrhoeal diseases: a systematic analysis for the Global Burden of Disease Study 2015. Lancet Infect Dis. 2017; 17:909–948. [PubMed: 28579426]

4. DuPont HL, Levine MM, Hornick RB, Formal SB. Inoculum size in shigellosis and implications for expected mode of transmission. J Infect Dis. 1989; 159:1126–1128. [PubMed: 2656880]
5. Kotloff KL, Nataro JP, Blackwelder WC, Nasrin D, Farag TH, Panchalingam S, Wu Y, Sow SO, Sur D, Breiman RF, Faruque AS, Zaidi AK, Saha D, Alonso PL, Tamboura B, Sanogo D, Onwuchekwa U, Manna B, Ramamurthy T, Kanungo S, Ochieng JB, Omore R, Oundo JO, Hossain A, Das SK, Ahmed S, Qureshi S, Quadri F, Adegbola RA, Antonio M, Hossain MJ, Akinsola A, Mandomando I, Nhampossa T, Acacio S, Biswas K, O'Reilly CE, Mintz ED, Berkeley LY, Muhsen K, Sommerfelt H, Robins-Browne RM, Levine MM. Burden and aetiology of diarrhoeal disease in infants and young children in developing countries (the Global Enteric Multicenter Study, GEMS): a prospective, case-control study. Lancet. 2013; 382:209–222. [PubMed: 23680352]
6. Kotloff KL, Winickoff JP, Ivanoff B, Clemens JD, Swerdlow DL, Sansonetti PJ, Adak GK, Levine MM. Global burden of Shigella infections: implications for vaccine development and implementation of control strategies. Bull World Health Organ. 1999; 77:651–666. [PubMed: 10516787]
7. Dutta S, Ghosh A, Ghosh K, Dutta D, Bhattacharya SK, Nair GB, Yoshida S. Newly emerged multiple-antibiotic-resistant *Shigella dysenteriae* type 1 strains in and around Kolkata, India, are clonal. J Clin Microbiol. 2003; 41:5833–5834. [PubMed: 14662996]
8. Anderson M, Sansonetti PJ, Marteyn BS. Shigella Diversity and Changing Landscape: Insights for the Twenty-First Century. Front Cell Infect Microbiol. 2016; 6:45. [PubMed: 27148494]
9. Galan JE, Lara-Tejero M, Marlovits TC, Wagner S. Bacterial type III secretion systems: specialized nanomachines for protein delivery into target cells. Annu Rev Microbiol. 2014; 68:415–438. [PubMed: 25002086]
10. Diepold A, Armitage JP. Type III secretion systems: the bacterial flagellum and the injectisome. Philos Trans R Soc Lond B Biol Sci. 2015:370.
11. Phalipon A, Sansonetti PJ. Shigella's ways of manipulating the host intestinal innate and adaptive immune system: a tool box for survival? Immunol Cell Biol. 2007; 85:119–129. [PubMed: 17213832]
12. Mueller CA, Broz P, Cornelis GR. The type III secretion system tip complex and translocon. Mol Microbiol. 2008; 68:1085–1095. [PubMed: 18430138]
13. Hu B, Morado DR, Margolin W, Rohde JR, Arizmendi O, Picking WL, Picking WD, Liu J. Visualization of the type III secretion sorting platform of Shigella flexneri. Proc Natl Acad Sci U S A. 2015; 112:1047–1052. [PubMed: 25583506]
14. Epler CR, Dickenson NE, Bullitt E, Picking WL. Ultrastructural analysis of IpaD at the tip of the nascent MxiH type III secretion apparatus of Shigella flexneri. J Mol Biol. 2012; 420:29–39. [PubMed: 22480614]
15. Cheung M, Shen DK, Makino F, Kato T, Roehrich AD, Martinez-Argudo I, Walker ML, Murillo I, Liu X, Pain M, Brown J, Frazer G, Mantell J, Mina P, Todd T, Sessions RB, Namba K, Blocker AJ. Three-dimensional electron microscopy reconstruction and cysteine-mediated crosslinking provide a model of the type III secretion system needle tip complex. Mol Microbiol. 2015; 95:31–50. [PubMed: 25353930]
16. Olive AJ, Kenjale R, Espina M, Moore DS, Picking WL, Picking WD. Bile salts stimulate recruitment of IpaB to the Shigella flexneri surface, where it colocalizes with IpaD at the tip of the type III secretion needle. Infect Immun. 2007; 75:2626–2629. [PubMed: 17296762]
17. Perwaiz S, Tuchweber B, Mignault D, Gilat T, Yousef IM. Determination of bile acids in biological fluids by liquid chromatography-electrospray tandem mass spectrometry. J Lipid Res. 2001; 42:114–119. [PubMed: 11160372]
18. Stensrud KF, Adam PR, La Mar CD, Olive AJ, Lushington GH, Sudharsan R, Shelton NL, Givens RS, Picking WL, Picking WD. Deoxycholate interacts with IpaD of Shigella flexneri in inducing the recruitment of IpaB to the type III secretion apparatus needle tip. J Biol Chem. 2008; 283:18646–18654. [PubMed: 18450744]

19. Dickenson NE, Zhang L, Epler CR, Adam PR, Picking WL, Picking WD. Conformational changes in IpaD from Shigella flexneri upon binding bile salts provide insight into the second step of type III secretion. Biochemistry. 2011; 50:172–180. [PubMed: 21126091]
20. Dickenson NE, Arizmendi O, Patil MK, Toth RTt, Middaugh CR, Picking WD, Picking WL. N-terminus of IpaB provides a potential anchor to the Shigella type III secretion system tip complex protein IpaD. Biochemistry. 2013; 52:8790–8799. [PubMed: 24236510]
21. Epler CR, Dickenson NE, Olive AJ, Picking WL, Picking WD. Liposomes recruit IpaC to the Shigella flexneri type III secretion apparatus needle as a final step in secretion induction. Infect Immun. 2009; 77:2754–2761. [PubMed: 19433542]
22. Dickenson NE, Picking WD. Forster resonance energy transfer (FRET) as a tool for dissecting the molecular mechanisms for maturation of the Shigella type III secretion needle tip complex. Int J Mol Sci. 2012; 13:15137–15161. [PubMed: 23203116]
23. Barta ML, Guragain M, Adam P, Dickenson NE, Patil M, Geisbrecht BV, Picking WL, Picking WD. Identification of the bile salt binding site on IpaD from Shigella flexneri and the influence of ligand binding on IpaD structure. Proteins. 2012; 80:935–945. [PubMed: 22423359]
24. Johnson S, Roversi P, Espina M, Olive A, Deane JE, Birket S, Field T, Picking WD, Blocker AJ, Galyov EE, Picking WL, Lea SM. Self-chaperoning of the type III secretion system needle tip proteins IpaD and BipD. J Biol Chem. 2007; 282:4035–4044. [PubMed: 17077085]
25. Cooley RB, Arp DJ, Karplus PA. Evolutionary origin of a secondary structure: pi-helices as cryptic but widespread insertional variations of alpha-helices that enhance protein functionality. J Mol Biol. 2010; 404:232–246. [PubMed: 20888342]
26. Riek RP, Graham RM. The elusive pi-helix. J Struct Biol. 2011; 173:153–160. [PubMed: 20828621]
27. Myers JK, Pace CN, Scholtz JM. Helix propensities are identical in proteins and peptides. Biochemistry. 1997; 36:10923–10929. [PubMed: 9283083]
28. Formal SB, Dammin GJ, Labrec EH, Schneider H. Experimental Shigella infections: characteristics of a fatal infection produced in guinea pigs. J Bacteriol. 1958; 75:604–610. [PubMed: 13538931]
29. Menard R, Sansonetti PJ, Parsot C. Nonpolar mutagenesis of the ipa genes defines IpaB, IpaC, and IpaD as effectors of Shigella flexneri entry into epithelial cells. J Bacteriol. 1993; 175:5899–5906. [PubMed: 8376337]
30. Andrade MA, Chacon P, Merelo JJ, Moran F. Evaluation of secondary structure of proteins from UV circular dichroism spectra using an unsupervised learning neural network. Protein Eng. 1993; 6:383–390. [PubMed: 8332596]
31. Whitmore L, Wallace BA. Protein secondary structure analyses from circular dichroism spectroscopy: methods and reference databases. Biopolymers. 2008; 89:392–400. [PubMed: 17896349]
32. Espina M, Olive AJ, Kenjale R, Moore DS, Ausar SF, Kaminski RW, Oaks EV, Middaugh CR, Picking WD, Picking WL. IpaD localizes to the tip of the type III secretion system needle of Shigella flexneri. Infect Immun. 2006; 74:4391–4400. [PubMed: 16861624]
33. Schiavolin L, Meghraoui A, Cherradi Y, Biskri L, Botteaux A, Allaoui A. Functional insights into the Shigella type III needle tip IpaD in secretion control and cell contact. Mol Microbiol. 2013; 88:268–282. [PubMed: 23421804]
34. Parsot C, Menard R, Gounon P, Sansonetti PJ. Enhanced secretion through the Shigella flexneri Mxi-Spa translocon leads to assembly of extracellular proteins into macromolecular structures. Mol Microbiol. 1995; 16:291–300. [PubMed: 7565091]
35. Kenjale R, Wilson J, Zenk SF, Saurya S, Picking WL, Picking WD, Blocker A. The needle component of the type III secreton of Shigella regulates the activity of the secretion apparatus. J Biol Chem. 2005; 280:42929–42937. [PubMed: 16227202]
36. Sansonetti PJ, Ryter A, Clerc P, Maurelli AT, Mounier J. Multiplication of Shigella flexneri within HeLa cells: lysis of the phagocytic vacuole and plasmid-mediated contact hemolysis. Infect Immun. 1986; 51:461–469. [PubMed: 3510976]
37. Niesel DW, Chambers CE, Stockman SL. Quantitation of HeLa cell monolayer invasion by Shigella and Salmonella species. J Clin Microbiol. 1985; 22:897–902. [PubMed: 4066921]

38. Picking WL, Picking WD. The Many Faces of IpaB. Front Cell Infect Microbiol. 2016; 6:12. [PubMed: 26904511]
39. Blocker A, Gounon P, Larquet E, Niebuhr K, Cabiaux V, Parsot C, Sansonetti P. The tripartite type III secreton of Shigella flexneri inserts IpaB and IpaC into host membranes. J Cell Biol. 1999; 147:683–693. [PubMed: 10545510]
40. Chatterjee S, Chaudhury S, McShan AC, Kaur K, De Guzman RN. Structure and biophysics of type III secretion in bacteria. Biochemistry. 2013; 52:2508–2517. [PubMed: 23521714]
41. Dickenson NE, Choudhari SP, Adam PR, Kramer RM, Joshi SB, Middaugh CR, Picking WL, Picking WD. Oligomeric states of the Shigella translocator protein IpaB provide structural insights into formation of the type III secretion translocon. Protein Sci. 2013; 22:614–627. [PubMed: 23456854]
42. Coburn B, Sekirov I, Finlay BB. Type III secretion systems and disease. Clinical microbiology reviews. 2007; 20:535–549. [PubMed: 17934073]
43. Cossart P, Sansonetti PJ. Bacterial invasion: the paradigms of enteroinvasive pathogens. Science. 2004; 304:242–248. [PubMed: 15073367]
44. Puhar A, Sansonetti PJ. Type III secretion system. Curr Biol. 2014; 24:R784–791. [PubMed: 25202865]
45. Deng W, Marshall NC, Rowland JL, McCoy JM, Worrall LJ, Santos AS, Strynadka NCJ, Finlay BB. Assembly, structure, function and regulation of type III secretion systems. Nat Rev Microbiol. 2017; 15:323–337. [PubMed: 28392566]
46. Pal M, Erskine PT, Gill RS, Wood SP, Cooper JB. Near-atomic resolution analysis of BipD, a component of the type III secretion system of Burkholderia pseudomallei. Acta Crystallogr Sect F Struct Biol Cryst Commun. 2010; 66:990–993.
47. Chaudhury S, Battaile KP, Lovell S, Plano GV, De Guzman RN. Structure of the Yersinia pestis tip protein LcrV refined to 1.65 A resolution. Acta Crystallogr Sect F Struct Biol Cryst Commun. 2013; 69:477–481.
48. Chatterjee S, Zhong D, Nordhues BA, Battaile KP, Lovell S, De Guzman RN. The crystal structures of the Salmonella type III secretion system tip protein SipD in complex with deoxycholate and chenodeoxycholate. Protein Sci. 2011; 20:75–86. [PubMed: 21031487]
49. Heinz DW, Baase WA, Dahlquist FW, Matthews BW. How aminoacid insertions are allowed in an alpha-helix of T4 lysozyme. Nature. 1993; 361:561–564. [PubMed: 8429913]
50. Keefe LJ, Sondek J, Shortle D, Lattman EE. The alpha aneurism: a structural motif revealed in an insertion mutant of staphylococcal nuclease. Proc Natl Acad Sci U S A. 1993; 90:3275–3279. [PubMed: 8475069]
51. Gibson RP, Turkenburg JP, Charnock SJ, Lloyd R, Davies GJ. Insights into trehalose synthesis provided by the structure of the retaining glucosyltransferase OtsA. Chem Biol. 2002; 9:1337–1346. [PubMed: 12498887]
52. Bailey LJ, McCoy JG, Phillips GN Jr, Fox BG. Structural consequences of effector protein complex formation in a diiron hydroxylase. Proc Natl Acad Sci U S A. 2008; 105:19194–19198. [PubMed: 19033467]
53. Wiersinga WJ, van der Poll T, White NJ, Day NP, Peacock SJ. Melioidosis: insights into the pathogenicity of Burkholderia pseudomallei. Nat Rev Microbiol. 2006; 4:272–282. [PubMed: 16541135]
54. McNally A, Thomson NR, Reuter S, Wren BW. ‘Add, stir and reduce’: Yersinia spp. as model bacteria for pathogen evolution. Nat Rev Microbiol. 2016; 14:177–190. [PubMed: 26876035]
55. Galan JE. Salmonella interactions with host cells: type III secretion at work. Annu Rev Cell Dev Biol. 2001; 17:53–86. [PubMed: 11687484]
56. Fabrega A, Vila J. Salmonella enterica serovar Typhimurium skills to succeed in the host: virulence and regulation. Clinical microbiology reviews. 2013; 26:308–341. [PubMed: 23554419]
57. Prouty AM, Brodsky IE, Falkow S, Gunn JS. Bile-salt-mediated induction of antimicrobial and bile resistance in Salmonella typhimurium. Microbiology. 2004; 150:775–783. [PubMed: 15073288]
58. Prouty AM, Gunn JS. Salmonella enterica serovar typhimurium invasion is repressed in the presence of bile. Infect Immun. 2000; 68:6763–6769. [PubMed: 11083793]

59. Prouty AM, Brodsky IE, Manos J, Belas R, Falkow S, Gunn JS. Transcriptional regulation of Salmonella enterica serovar Typhimurium genes by bile. FEMS Immunol Med Microbiol. 2004; 41:177–185. [PubMed: 15145463]

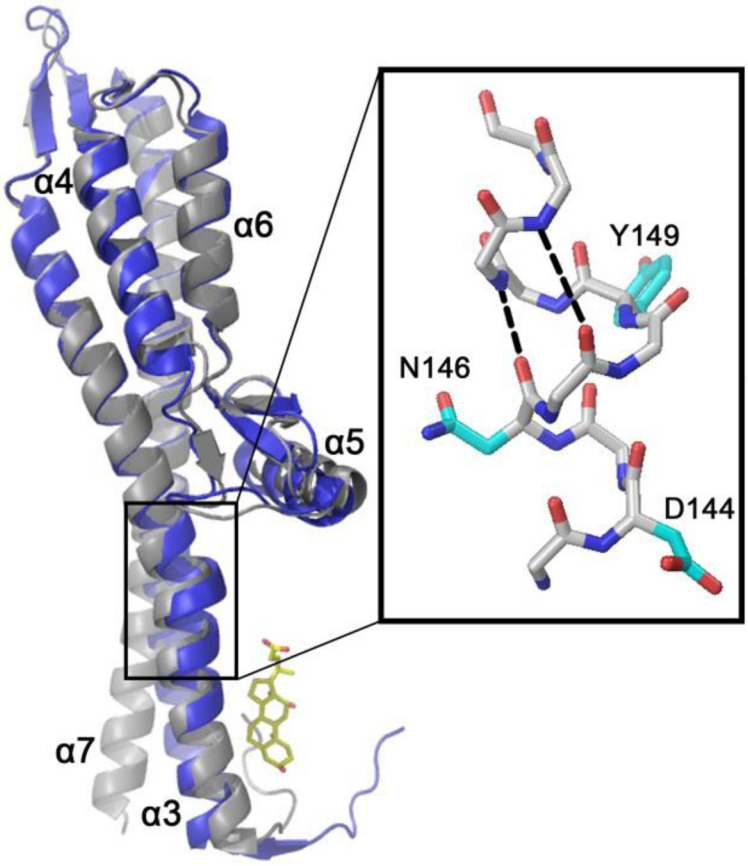


**Figure 1. A π-helix supports DOC-induced conformational changes in IpaD**

An overlay of apo- (gray) and DOC-bound (blue) crystal structures of IpaD identifies the DOC binding site (DOC in yellow) as well as regions of the protein that undergo significant conformational changes upon binding. The π-helix within α3 is identified by a black box and the peptide backbone of the corresponding region is shown to the right with carbon, oxygen, and nitrogen atoms represented in gray, blue, and red, respectively. The sidechains targeted for mutation are shown in cyan and the i+5 hydrogen bonds supporting the π-helix are depicted by dashed lines. This figure was generated using PyMol[1] and the PDB files 2J0O and 3R9V for the apo- and DOC bound IpaD structures, respectively. The proximal domain containing helices α1 and α2 was removed from 2J0O for clarity. The coordinates from 3R9V were used to generate the peptide backbone view.

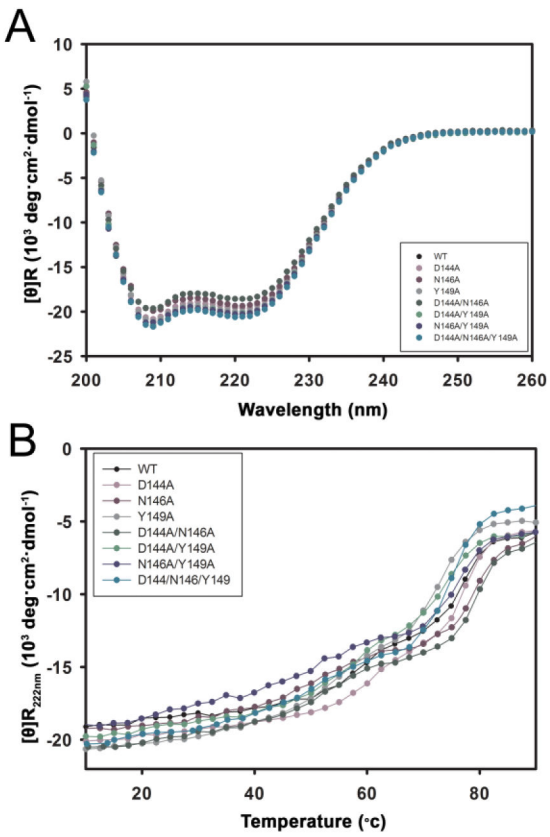


**Figure 2. Engineered IpaD π-helix mutants maintain native secondary structure content and stability**

**A)** Far-UV CD spectra of all the IpaD mutant proteins are similar to that of wild-type IpaD with minima observed at 208 and 222 nm, consistent with predominantly α-helical secondary structure. **B)** Thermal unfolding of the secondary structures of IpaD and the IpaD π-helix mutants is observed by plotting the mean residue molar ellipticity at 222 nm while the protein solutions are heated from 10 to 90 °C. All CD measurements were collected at 0.3 – 0.6 mg/mL IpaD concentrations with the displayed data representative of triplicate measurements of at least two biological replicates.

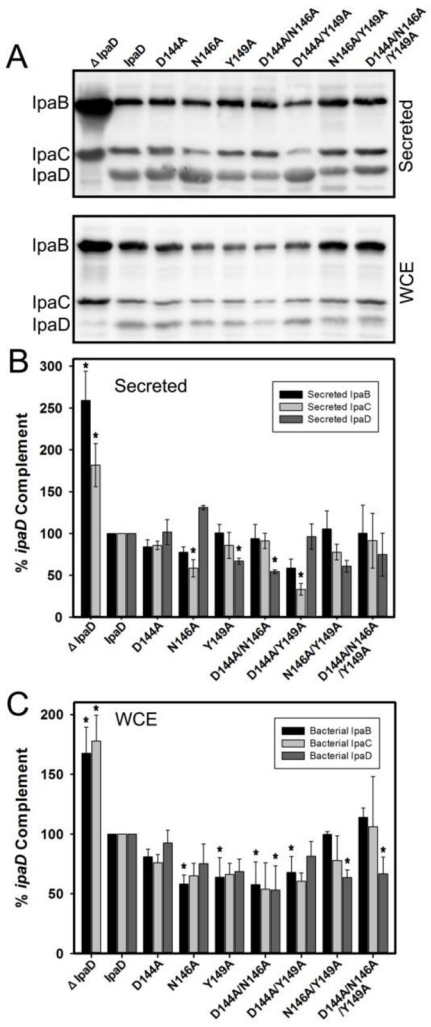


**Figure 3. Basal secretion of IpaB and IpaC is impacted by mutations in the IpaD π-helix**

**A)** Representative western blot of the protein secreted through the T3SS into growth media (top) and remaining in the whole cell extract (bottom) by ΔIpaD *Shigella* strains complemented with the indicated IpaD variants. The western blot intensities for each secreted protein were quantified relative to wild-type IpaD and plotted as the average relative protein levels recovered from the culture media **(B)** and remaining within in the whole cell extract (WCE) **(C)** from 3 independent secretion experiments. * Indicates a significant difference in the detected protein level relative to the wild-type *ipaD* complement strain (one-way ANOVA followed by a Dunnett's post test, $p \leq 0.01$)).

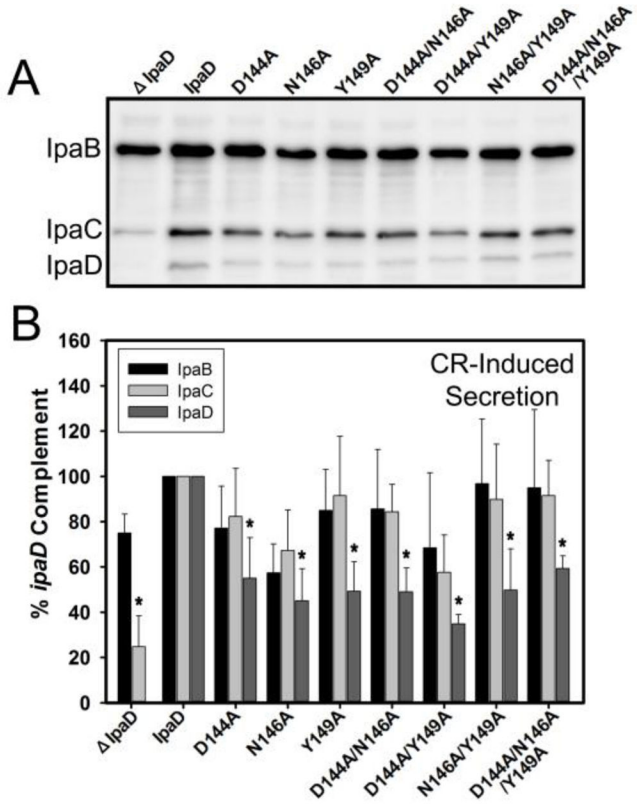


**Figure 4. Congo red-induced active secretion of IpaB and IpaC is unaffected by IpaD π-helix mutations**

**A)** Representative western blot of secreted IpaB, IpaC, and IpaD following Congo red exposure to the ΔIpaD *Shigella* strain and those complemented with the indicated IpaD variants. **B)** The western blot intensities resulting from actively secreted IpaB, IpaC, and IpaD were quantified and plotted as the average ± standard deviation from three independent analyses. The quantified protein levels are displayed as a percentage relative to those secreted by the *Shigella* strain expressing wild-type IpaD. * Indicates a significant difference in the detected protein level relative to the wild-type *ipaD* complement strain (one-way ANOVA followed by a Dunnett's post test, $p \leq 0.01$)).

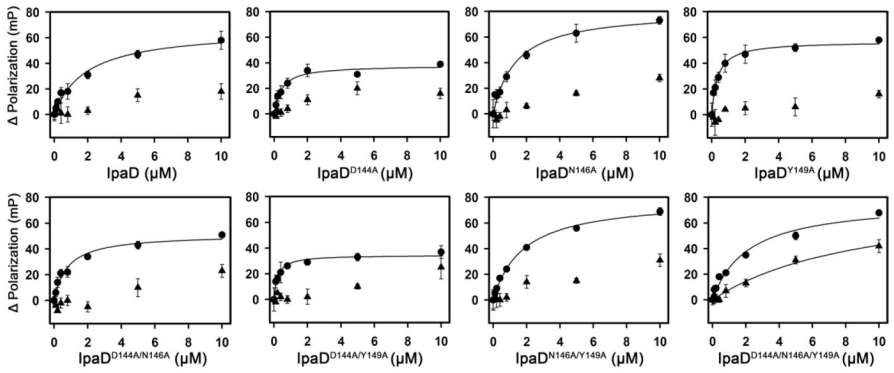


**Figure 5. Engineered IpaD π-helix mutations alter DOC-dependence on IpaD-IpaB interactions**

Polarization assays were carried out both in the absence (closed triangles) and presence (closed circles) of 1 mM deoxycholate. The results were fit to a single site saturation model and only fits resulting in a $R^2 \geq 0.95$ were overlaid on the binding data. Each graph was generated from triplicate technical replicates and is representative of a minimum of three independent experimental analyses used to determine the apparent binding affinity for each condition. Error bars represent standard deviation around the mean at each data point.

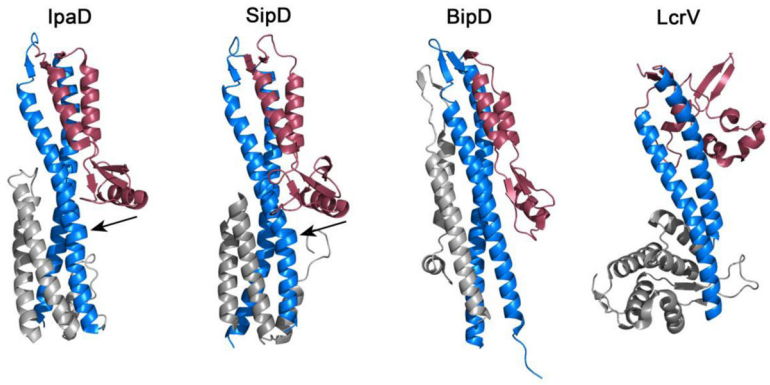


**Figure 6. *Shigella* IpaD and *Salmonella* SipD exhibit rare π-helices**

The central coiled coil, distal domain and proximal domain in each protein is shown in blue, red, and gray, respectively. The π-helices in IpaD and SipD are found in similar regions of the proteins and are indicated by black arrows. Though overall structurally similar to IpaD and SipD, BipD and LcrV both lack π-helices in their structures. The structures were generated using PyMol and the PDB coordinates from 2J0O, 3NZZ, 3NFT, and 4JBU for IpaD from *Shigella flexneri*, SipD from *Salmonella enterica* serovar Typhimurium, BipD from *Burkholderia pseudomallei*, and LcrV from *Yersinia pestis*, respectively.

## Table 1

Measured binding affinities between engineered IpaD π-helix mutants and the bile salt deoxycholate

| IpaD Mutant | $K_d$ (μM) ± SD[a] |
|---|---|
| Wild-type IpaD | 9.3 ± 1.8 |
| D144A | 10.5 ± 2.5 |
| N146A | 10.9 ± 0.2 |
| Y149A | 10.8 ± 0.3 |
| D144A/N146A | 9.7 ± 1.7 |
| D144A/Y149A | 10.7 ± 1.5 |
| N146A/Y149A | 9.9 ± 2.3 |
| D144A/N146A/Y149A | 8.3 ± 2.2 |

[a]Apparent $K_d$ values between IpaD and fluorescein-DOC reported as the mean ± standard deviation resulting from three independent analyses. There is no statistical difference among the means (one-way ANOVA ($F(7,16) = 0.803$, $p = 0.597$)).

## Table 2

Effect of engineered IpaD π-helix mutations on *Shigella* hemolysis and invasion phenotype

| | Hemolysis[a] | Invasion[b] | |
|---|---|---|---|
| **IpaD Mutant** | **(%WT ± SD)** | **−DOC (%WT ± SD)** | **DOC response (%change ± SD)** |
| ΔIpaD | 2.1 ± 0.2 * | 0 ± 0 * | 0 ± 0 * |
| Wild-type IpaD | 100.0 ± 2.2 | 100 ± 0 | 83 ± 14 |
| D144A | 80.3 ± 9.1 | 142 ± 28 * | 88 ± 26 |
| N146A | 70.6 ± 10.4 | 78 ± 25 * | 50 ± 35 * |
| Y149A | 88.1 ± 2.9 | 93 ± 16 | 75 ± 21 |
| D144A/N146A | 82.2 ± 16.9 | 103 ± 24 | 75 ± 28 |
| D144A/Y149A | 88.4 ± 9.4 | 85 ± 38 | 39 ± 15 * |
| N146A/Y149A | 85.8 ± 5.7 | 68 ± 7 * | 83 ± 37 |
| D144A/N146A/Y149A | 92.5 ± 7.0 | 107 ± 36 | −28 ± 20 * |

[a] Hemolysis results are presented as a percentage of the hemoglobin released from red blood cells by the ΔIpaD *S. flexneri* strain complemented with wild-type IpaD.

[b] Invasion results are presented as a percentage of the number of colonies resulting from the ΔIpaD *S. flexneri* strain complemented with wild-type IpaD in the absence of DOC and as a percent change in invasion for each strain following DOC exposure. All data result from a minimum of three independent analysis with the results presented as the mean ± standard deviation.

* Indicates statistical difference from the wild-type IpaD complement strain tested under identical conditions (one-way ANOVA followed by a Dunnett's post test, $p \leq 0.01$)).

## Table 3

Effect of DOC on the binding affinity between engineered IpaD π-helix mutants and IpaB$^{28–226}$

| | $K_d$ (μM ± SD) [a,b] | |
|---|---|---|
| **IpaD Mutant** | **− DOC** | **+ DOC** |
| Wild-type IpaD | - | 2.0 ± 0.7 |
| D144A | - | 0.4 ± 0.2 * |
| N146A | - | 1.4 ± 0.3 * |
| Y149A | - | 0.5 ± 0.3 * |
| D144A/N146A | - | 0.6 ± 0.2 * |
| D144A/Y149A | - | 0.3 ± 0.2 * |
| N146A/Y149A | - | 2.1 ± 0.6 |
| D144A/N146A/Y149A | 7.4 ± 2.4 | 2.2 ± 0.8 |

[a] Apparent dissociation constants between IpaD and IpaB$^{28–226}$ are reported as the mean ± standard deviation resulting from at least three independent analyses.

[b] $K_d$ values are only reported for conditions resulting in fits with $R^2$ values ≥ 0.95.

* Indicates statistical difference from the wild-type IpaD complement strain (one-way ANOVA followed by a Dunnett's post test, $p \leq 0.01$)).